Agent-Based Computational Modeling of Wounded Epithelial Cell Monolayers

D. C. Walker, G. Hill, S. M. Wood, R. H. Smallwood, and J. Southgate*

***Abstract*—Computational modeling of biological systems, or *in silico* biology, is an emerging tool for understanding structure and order in biological tissues. Computational models of the behavior of epithelial cells in monolayer cell culture have been developed and used to predict the healing characteristics of scratch wounds made to urothelial cell cultures maintained in low- and physiological [Ca^{2+}] environments. Both computational models and *in vitro* experiments demonstrated that in low exogenous [Ca^{2+}], the closure of 500-μm scratch wounds was achieved primarily by cell migration into the denuded area. The wound healing rate in low (0.09 mM) [Ca^{2+}] was approximately twice as rapid as in physiological (2 mM) [Ca^{2+}]. Computational modeling predicted that in cell cultures that are actively proliferating, no increase in the fraction of cells in the S-phase would be expected, and this conclusion was supported experimentally *in vitro* by bromodeoxyuridine incorporation assay. We have demonstrated that a simple rule-based model of cell behavior, incorporating rules relating to contact inhibition of proliferation and migration, is sufficient to qualitatively predict the calcium-dependent pattern of wound closure observed *in vitro*. Differences between the *in vitro* and *in silico* models suggest a role for wound-induced signaling events in urothelial cell cultures.**

***Index Terms*—Calcium, computational modeling, emergent structure, urinary epithelium, wound healing.**

I. Introduction

EPITHELIAL tissues are structured and highly organized self-renewing communities of cells that form the interface with the external environment and show morphological and molecular specializations reflecting tissue type-specific barrier, absorptive and secretory functions. Epithelial tissues are implicated in the etiology of many human diseases, and most significantly, >85% of adult human malignancies are carcinomas of epithelial cell origin. However, little is known of the underlying tissue regulatory mechanisms that, for example, control tissue architecture and regulate the balance between cell proliferation, differentiation, and apoptosis. We have been investigating some of these issues in the transitional-type epithelium ("urothelium") that lines the bladder and associated urinary tract. Urothelium is a stratified epithelium that functions to provide a low-permeability barrier to urine, while accommodating changes in bladder volume. This specialized function is reflected in the expression of urothelium-specific gene products by the terminally differentiated superficial cells. *In vivo*, urothelium proliferates extremely slowly, with a turnover time of approximately one year, but has a high proliferative capacity in response to injury. The effective wound response has presumably evolved to ensure rapid reinstatement of the urinary barrier.

Our experimental strategy has been to develop *in vitro* cell culture systems to investigate the biology of human urothelium. We have established methods to isolate and propagate normal human urothelial (NHU) cells in serum-free medium in monoculture, where they can be serially passaged as finite cell lines [1], [2]. The NHU cell lines grow as monolayers and adopt the highly proliferative and migratory phenotype of a urothelial "wound response" [3]. The NHU cell lines can be induced to express genes associated with terminal urothelial differentiation [4] and, when transplanted onto an urothelial stroma maintained in organotypic culture, will stratify and form a histologically normal urothelium [5]. The ability of *in vitro*-propagated urothelial cells to differentiate and form a urothelial tissue is important evidence toward validating the urothelial cell culture system, as it implies that urothelial cells are not compromised upon isolation from the tissue, but rather that the phenotype reflects a normal response to the cell culture environment.

The capacity for urothelial cells to self-organize into an urothelial tissue structure appears to be an emergent property of the way in which cells interact with each other and with the substrate. We have termed these interactions the "social behavior" of cells and have developed an agent-based computational model to test the hypothesis that population-based or "tissue" behavior is accountable by cell-based rules of physical engagement between neighbors.

Computational modeling is a tool of growing importance in biology, providing an insight into the complexity of systems that scale orders of magnitude in time and space and predicting the outcome of multiple interactions across these scales. Whereas many computational models in biology and medicine predict function or physical properties as a result of structure, we have developed a modeling system that predicts growth patterns in a virtual cell culture environment as a result of interactions between individual cells. At this stage, our model considers only two-dimensional (2-D) cellular interactions. However, this simple model allows us to examine the hypothesis that

Manuscript received January 7, 2004; revised April 28, 2004. This work was supported by the Engineering and Physical Sciences Research Council (EPSRC) under Platform Grant GR/R48032. The work of G. Hill was supported on a studentship from the Biotechnology and Biological Sciences Research Council and Smith & Nephew plc. The work of J. Southgate was supported by York Against Cancer. *Asterisk indicates corresponding author.*

D. C. Walker and R. H. Smallwood are with the Department of Computer Science, University of Sheffield, Sheffield S1 4DP, U.K.

G. Hill is with the Jack Birch Unit of Molecular Carcinogenesis, Department of Biology, University of York, York YO10 5YW, U.K.

S. M. Wood is with the Sheffield Teaching Hospitals, NHS Foundation Trust, Sheffield S10 2JF, U.K.

*J. Southgate is with the Jack Birch Unit of Molecular Carcinogenesis, Department of Biology, University of York, York YO10 5YW, U.K. (e-mail: js35@york.ac.uk).

Digital Object Identifier 10.1109/TNB.2004.833680

it is the interactions between individual cells that govern the growth characteristics of a cell population. In this paper, we present a direct comparison between computational model predictions in the context of healing of a scratch wound in a confluent monolayer with experimental results obtained from the equivalent *in vitro* system.

A. Agent-Based Computational Modeling of Biological Cells

The model we have developed, the *Epitheliome*, considers each virtual cell as an entity governed by a number of simple rules, for instance, relating to cell cycle regulation or calcium-dependent bonding affinities. Hence, we can predict how organization in the model, determined by relationships between individual cells, evolves with time. Like the biological cells that they represent, our virtual cells are able to progress through the cell cycle, form bonds with one another and the virtual substrate, migrate, change shape, divide, or die. We have already used this model to predict how patterns of growth are modulated by exogenous [Ca^{2+}] concentration [6], and in this paper we extend the model to predict the healing of wounded confluent monolayers in different calcium ion concentrations. Specifically, we aim to determine which aspects of wound closure can be predicted using a combination of physical and simple rules representing cell behavior and to identify biological phenomena currently missing from the model that could be incorporated in the future.

B. Effect of Exogenous Calcium Concentration

The proliferation or differentiation of cells *in vitro* can be affected by a number of factors, including choice of culture substrate, growth factors, and exogenous [Ca^{2+}]. Studies on the effect of exogenous [Ca^{2+}] have shown that in conditions of low [Ca^{2+}], epithelial cells proliferate more rapidly and do not form desmosomes. Increasing the calcium ion concentration of the culture medium results in rapid desmosome formation, stratification, and differentiation [1], [7], [8]. Magee *et al.* observed that keratinocytes in low [Ca^{2+}] were more motile and migrated into a wound created in a cultured monolayer, whereas those maintained in physiological [Ca^{2+}] did not [9]. Interestingly, Jensen *et al.* observed that lateral growth was retarded in low exogenous [Ca^{2+}], but also noted an increase in thymidine incorporation, indicating rapidly cycling cells [10].

In the NHU cell culture system referred to here, the cells are routinely cultured in medium containing subphysiological (0.09 mM) [Ca^{2+}], in order to maximize proliferation. In this case, addition of exogenous calcium to the medium results in desmosome formation and cell stratification, but does not induce terminal urothelial differentiation [1].

The exact mechanism of calcium-mediated inhibition of growth remains controversial. The membrane-bound adhesion protein E-cadherin requires the presence of calcium ions in order to form intercellular adherens junctions. This protein is also linked to growth-related signaling pathways. Proposed mechanisms for E-cadherin-mediated inhibition of proliferation include up-regulation of the cyclin-dependent kinase inhibitor p27 [11], translocation of the transcription factor β-catenin to the cell membrane [12], or the interference of intercellular bonds with activation of the epidermal growth factor (EGF) receptor [13]. As well as influencing proliferation and differentiation in cell culture, E-cadherin also affects cell motility, and its down-regulation has been linked to tumor invasion [14]. The multiple effects of exogenous [Ca^{2+}] on cell behavior lead us to expect a difference in the rate of wound closure in cultured urothelium. Specifically, we predict that changes in the way cells interact in low- versus high-[Ca^{2+}] environments will lead to predictive differences in the rate and mechanisms of scratch wound closure.

II. Methods

A. Computational Modeling of Monolayer Wounding

A detailed description of the computational modeling program *Epitheliome* is available elsewhere [6]. Briefly, the model consists of a number of cells interacting with their environment, which comprises a 2-D square substrate with user-defined dimensions and modifiable exogenous [Ca^{2+}]. The user can select the number of cells seeded and whether to place them randomly on the substrate or in specified locations. The seed cell radii and other parameters such as mean cycle time and migration rate can be selected by the user and scaled so each model iteration represents approximately 30 min of real time. The software is coded in the Matlab software package.[1]

At each iteration, or tick of the model clock, each cell is interrogated in turn, and depending on the state of its internal parameters (e.g., current position in cell cycle, flag indicating attachment to substrate) and its environment (number and proximity of neighboring cells, concentration of calcium ions) a number of rules are executed that may change the state of the cell's internal parameters. During this process, cells can receive messages from other cells in their immediate vicinity or send messages to other cells by reading from and writing to a structure designated as a communication matrix. An additional global data structure, which can be accessed by all cells in the model, contains information relating to the exact position and dimensions of every cell. Thus, each cell "knows" the location (distance and azimuth) of its close neighbors within approximately ten cell radii and can moderate its behavior accordingly. This information is updated every time a cell moves or changes shape. If a cell divides during the simulation, one daughter cell overwrites the data structure of the parent, while the second daughter is added to end of the string of existing cell structures. A summary of the rules particularly relevant to the study outlined in this paper is given in Table I and Fig. 1.

As shown in the table, progression of a cell through the G1-G1/G0 checkpoint is dependent on two factors. First, if a cell has four or more intercellular bonds, it becomes contact inhibited and enters the G0 phase until one or more of these bonds are broken. Second, cells that have a radius less than 1.5 times that of their initial spherical radius at seeding also enter G0 until they have spread sufficiently to continue in G1 phase. This "size inhibition rule" is based on the observations of Nelson and Chen that endothelial cells with a surface area of greater than 1000 μm^2 exhibited significantly greater levels of bromodeoxyuridine (BrdU) incorporation than cells allowed

[1]Mathworks Inc. [Online]. Available: http://www.mathworks.com

TABLE I
MODEL RULES RELATING TO CELL CYCLE PROGRESSION

CURRENT STATE		ACTION
Cell is in G1		Increase cell volume by set amount Increment internal counter by +1
Cell is at G1/G0 check-point	If cell is bonded to 4 or more neighbors	Enter G0
	If cell is not sufficiently spread (radius < 1.5x 'rounded' radius)	
	ELSE	Continue in G1
Cell is in G0	If cell is bonded to less than 4 neighbors	Re-enter G1
	If cell sufficiently spread	
	ELSE	Remain in G0
Cell is in S/G2		Increment internal counter by +1
Cell is at G2/M boundary		Change to mitotic cell type
Cell is at end of M phase		Divide to create two identical daughter cells.

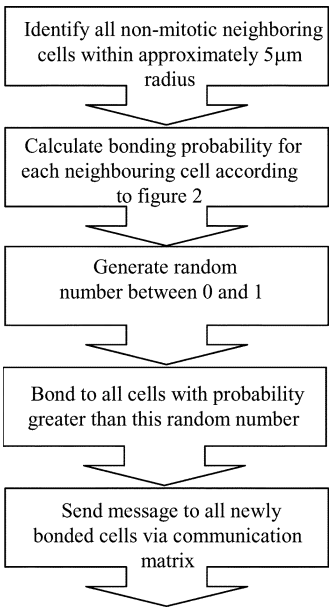

Fig. 1. Sequence of model rules relating to intercellular bonding.

to spread to less than half this area (or approximately 1.5 times smaller radius) [15].

Fig. 2 shows the relationship used to calculate the probability of neighboring cells bonding dependent on their edge separation and the exogenous [Ca^{2+}]. Cells are permitted to attempt to bond with neighbors within 5 μm of separation, which accounts for the tendency of biological cells to extend lamellapodia over a small distance in order to form initial attachments during the cell adhesion process [16]. The probability of any pair of model cells bonding is inversely proportional to the separation between the cell edges and related to the exogenous [Ca^{2+}] via a sigmoid function with the inflection point at 1.0 mM. This relationship is based on published data [17] on the relationship

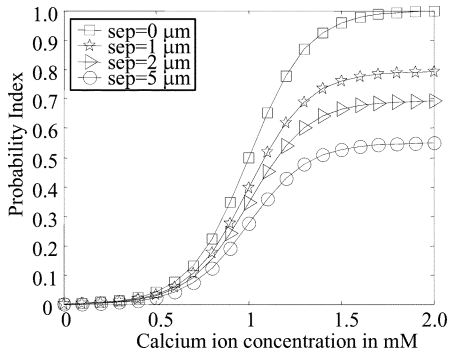

Fig. 2. Relationship between bonding probability, exogenous [Ca^{2+}] and separation between cell edges used in computational model.

between the binding activity of E-cadherin-mediated bonds and exogenous [Ca^{2+}]. This study used atomic force microscopy techniques to show that the presence of extracellular calcium ions is required for homotypic dimerization of E-cadherin. At low-[Ca^{2+}] concentrations, E-cadherin remains as a globular monomer and cannot interact to form adhesion bonds. The choice of an inflection point of 1.0 mM for the calculation of bond probability is also supported by the observations of [7] that 1.2 mM [Ca^{2+}] is required for the rapid formation of desmosomes and inhibition of proliferation in keratinocytes and those of [1] that switching of growth medium from 0.09 to 0.9 mM [Ca^{2+}] induced a significant change in morphology and growth characteristics in seven out of nine urothelial cell lines. However, this sigmoidal relationship does not account for the observation that in confluent cultures, bonds can be formed even in a low-[Ca^{2+}] environment, although these may be weaker and more transient than those formed in high [Ca^{2+}]. For this reason, as the model cell population approaches confluence, and individual cells experience crowding, a new rule is introduced that modifies the simple sigmoidal function to increase the probability of bonding, even in very low-[Ca^{2+}] conditions, to approximately one in three. For exogenous [Ca^{2+}] >1 mM, the probability index is greater than one, so crowded cells in contact will always form bonds under these circumstances.

After the rule sets have been applied to every cell in the model in turn, a numerical technique is then used to correct for any overlap between neighboring cells that may have resulted from cell growth, spreading, or division during the previous agent-based iteration. This involves identifying any overlap between every pair of neighboring cells in the model and applying a force proportional to this overlap to separate these cells. Cells which are bonded but separated by a small distance feel an attractive force. This is intended to simulate the role of lamellapodia in drawing two neighboring cells into contact as adhesion progresses [16]. Following the application of the numerical technique to attempt to equilibriate these repulsive and attractive forces, any intercellular bonds where the distance of separation remains greater than 1 μm are automatically broken. There is also a probability of spontaneous bond rupture for smaller but positive separations, which increases exponentially with separation and is inversely proportional to the exogenous [Ca^{2+}]. This rule reflects the transient nature of intercellular bonds, particularly in low exogenous [Ca^{2+}] conditions. For further details

on the implementation of the numerical technique, and rules relating to other aspects of cell behavior, see [6].

Two sets of computational simulations were undertaken: in the first case, the exogenous [Ca^{2+}] was set to 0.09 mM, and in the second set, this parameter was specified to be 2.0 mM (approximately physiological). The model substrate size was set at 1.2 by 1.2 mm and the number of cells seeded at the start of the simulation was 100, giving an initial seeding density of approximately 7×10^3 cells/cm^2. The cell cycle times in the model were set to 15 h, or 30 model iterations, and cell migration speed was set to approximately 1 μm/min, or 30–40 μm/iteration. Initially, simulations of cell population growth were carried out by applying the agent rules and simple physics interactions, described above, to the seeded cell populations. At every iteration, statistics relating to the state of the cell population (e.g., total cell number, number of cells with bonds, number of cells in different phases of the cell cycle) were saved for future reference. It is also possible to save the entire model, including the data structures representing every individual cell, at arbitrary points during the simulation, allowing the model to be restarted later at that particular time point. In order to investigate the effect of population quiescence on the response to wounding, models were saved for future wounding simulations at different stages of confluence/quiescence. In the case of the 0.09-mM [Ca^{2+}] model, cell populations were saved after 120 iterations (12% cells quiescent), 130 iterations (25% cells quiescent), and 140 iterations (50% cells quiescent). In the case of 2-mM [Ca^{2+}] simulations, cell populations were saved at 140 iterations (54% quiescence), 150 iterations (66% quiescence), and 160 iterations (75% quiescence). It was impractical to save low and physiological [Ca^{2+}] simulations with identical characteristics due to the different nature of population growth in the two environments. For instance, cells in the physiological [Ca^{2+}] model tend to form many intercellular bonds, grow in colonies, and become contact inhibited (i.e., enter G0) more quickly than in the low-[Ca^{2+}] model, so higher levels of quiescence are attained before the population reaches confluence (see [6] for details). As well as saving data at intermediate stages, both low and physiological calcium growth models were run until approximately 90% of the cells in the population were in G0. The data produced by these models, thus, provided a useful "control" for comparison with data produced in the wound model.

Scratch wounds were simulated in the saved models by removing all cells located within a 500-μm-wide strip in the center of the substrate. The models were then restarted and run for at least a further 40 iterations (20 h). Details of all models are summarized in Table II. As well as population statistics, image files of the substrate and cells were saved in JPEG format to allow visualization of the simulated wound healing.

TABLE II
DETAILS OF COMPUTATIONAL MODELS

Name	Ca^{2+} in mM	Wnd Y/N?	Start it. no.	End it. no.	Start cell no.	End cell no.	Start % G0	End % G0
L0	0.09	N	0	156	100	2862	0	89
LW1	0.09	Y	120	170	1583	2635	12	64
LW2	0.09	Y	130	170	1960	2604	25	29
LW3	0.09	Y	140	180	2452	2601	50	48
P0	2.0	N	0	178	100	2438	0	88
PW1	2.0	Y	140	190	1803	1667	54	73
PW2	2.0	Y	150	200	2024	1759	66	78
PW3	2.0	Y	160	200	2218	1651	75	81

Abbreviations: Wnd—wound model; it. no.—model iteration number)

TABLE III
ORIGINAL WIDTHS OF WOUNDS CREATED IN NHU CELL LINE Y358

	0.09mM [Ca^{2+}]			2.0mM [Ca^{2+}]		
Wound No.	1	2	3	1	2	3
Width in μm	456	700	751	616	773	756

B. In Vitro Wounding Assays

Specimens of normal adult and pediatric bladder, ureter, and renal pelvis were obtained during open urological surgery for nonneoplastic conditions and from patients undergoing nephrectomy for renal cell carcinoma. The collection of surgical specimens was approved by the relevant Local Research Ethics Committees and, where required, had full patient consent. Excised tissues were placed immediately into "transport medium" consisting of Hanks' balanced salt solution (HBSS) supplemented with 10 mM 4-(2-Hydroxyethyl)piperazine-1-ethanesulfonic acid (HEPES) pH 7.6 and 20 Kallikrein inactivating units (KIU)/mL aprotinin (Trasylol, Bayer, Newbury, U.K.), for transport to the laboratory. The urothelium was isolated from the underlying stromal tissue and established in culture as finite cell lines, as previously detailed [1], [2]. Briefly, the urothelium was detached from the underlying stroma by incubation at 4 °C in transport medium containing 0.1% (w/v) ethylenediaminetetraacetic acid (EDTA), incubated for 10 min at 37 °C in 200 U/mL collagenase type IV (Sigma). Urothelial cells were collected by centrifugation and seeded into Primaria tissue culture vessels. Growth medium consisted of keratinocyte serum-free medium (KSFM) containing 50 mg/mL bovine pituitary extract and 5 ng/mL EGF, as recommended by the manufacturer (Invitrogen Ltd., Paisley, U.K.), and 30 ng/mL cholera toxin (Sigma, Poole, U.K.). The KSFM medium with supplements will be referred to as KSFMC. Cells were harvested from the substrate by incubation in 0.1% (w/v) EDTA followed by trypsinization, as previously detailed [2].

1) Visual Recording of Wound Closure: Two independent normal human urothelial (NHU) cell lines that had each been subcultured four times were used for experiments described here.

Cells from NHU cell line Y358 were seeded into Primaria six well plates at a density of 10^4 cells/cm^2. Approximately two days after cells had reached confluence, the [Ca^{2+}] of the medium in half the wells was increased from 0.09 to 2 mM, by the addition of $CaCl_2$. After 72 h further incubation, scratch wounds were made across the center of each 3.5-cm-diameter well, using a 500-μm-wide sterile pipette tip. Cultures were washed in KSFMC (at the appropriate [Ca^{2+}]) to remove debris, and incubated for up to a further 24 h.

Migration of cells into the wound space was analyzed from digital phase contrast micrographs recorded at 60-min intervals from three replicate wells for both high- and low-calcium

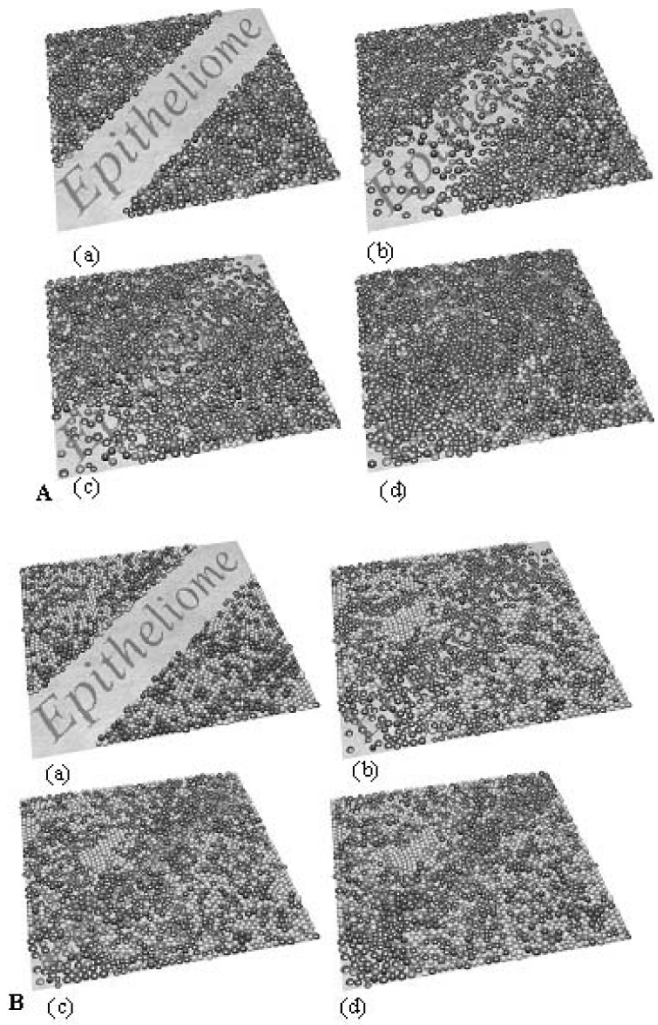

Fig. 3. Images of low-calcium computational model. (A) Model LW1 and (B) model LW3 at: (a) 0 h; (b) 3 h; (c) 6 h; (d) 9 h after wounding (dark cells—actively cycling, light cells—in G0).

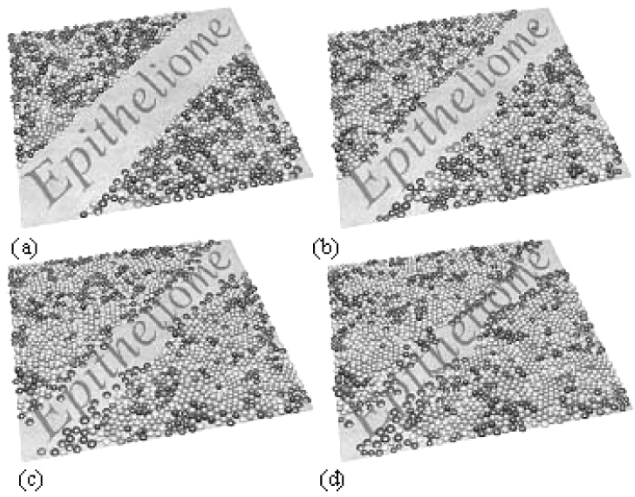

Fig. 4. Images of low-calcium computational model PW1 at: (a) 0 h; (b) 8 h; (c) 16 h; and (d) 24 h after wounding (dark cells—actively cycling, light cells—in G0).

media, starting from 30 min, until 13.5 h postwounding. A further image was obtained for each replicate approximately 24 h postwounding. Care was taken to photograph the same field at each time point, although in practice, some offset between fields was unavoidable. The digital images were loaded into Matlab, and the position of the wound edges at the zero time point (30 min postwounding) was obtained for each well and marked on all the images obtained for that well at subsequent time points. The number of cells within this area in each image was then counted manually and recorded, to provide an estimate of the rate of wound closure. Some variation was found in the original width of the wounds, due to difficulties in controlling the amount of pressure applied to the pipette tip during wounding. Original wound widths are given in Table III. In order to check reproducibility between cell lines, photomicrographs were also obtained for a series of time points between 0 and 9 h postwounding for a second independent NHU cell line, Y388.

2) BrdU Immunofluorescence: Incorporation of BrdU into DNA during the "S" or synthetic phase of the cell cycle was used to indicate cell proliferation in the monolayers after scratch wounding. Passage 3 NHU cells were seeded in 2 mL KSFMC at 2×10^5 cells/cm^2. Three hours after seeding, monolayers were washed to remove any unattached cells and plates were incubated in KSFMC containing 0.09 or 2 mM $CaCl_2$ for a further two days. Scratch wounds of approximately 500-μm width were created, as described above, in each of eight dishes containing low (0.09 mM), and near physiological (2 mM) [Ca^{2+}].

Immediately after washing, culture medium was aspirated from one wounded and one nonwounded control from both the low and physiological calcium sets, and BrdU labeling medium was added. The dishes were incubated for 6 h, fixed in ethanol: glycine fixative (three parts 50 mM glycine solution: seven parts absolute ethanol) and stored at -20 °C for analysis at a later date. This was repeated at a further seven time points of 6, 12, 18, 24, 30, 36, and 42 h postwounding.

Labeling of the fixed wells was carried out as follows: plates were washed three times in phosphate-buffered saline (PBS) to remove all traces of fixative. Anti-BrdU monoclonal antibody (Roche) was applied to each of the plates, which were incubated for 30 min at 37 °C. After three more washes, plates were incubated with fluorescein-conjugated antimouse secondary antibody for 30 min and washed with PBS. Cell nuclei were counterstained with a DNA intercalating dye by the application of 0.1 mg/mL Hoechst 33 258 for 5 min.

Each plate was viewed and analyzed using an epifluorescence microscope with digital camera (Olympus BX60). Cell counts of Hoechst 33 258 and BrdU labeled cells were obtained for at least six fields per well. A DNA synthesis index was calculated for each field of view by dividing the number of BrdU-positive nuclei by the total number of Hoechst 33 258-stained nuclei. Particle counting was carried out using a semiautomated process in the Matlab package. In order to eliminate any chance of bias and to ensure consistency, all BrdU images were analyzed "blind."

The replicate fields were used to generate a mean and standard deviation of the proliferative index for each of wells, at each of the sampled time points.

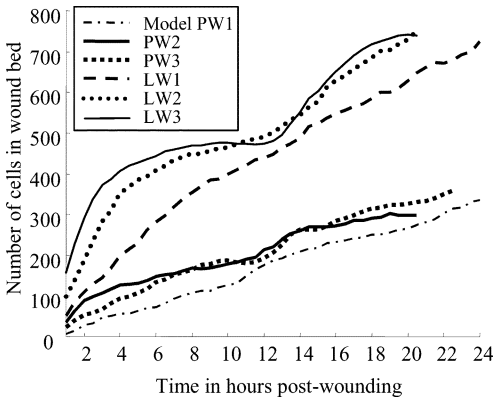

Fig. 5. Number of cells located within original wound area in computational models.

III. Results

A. Computational Modeling

1) Cell Migration: A selection of the JPEG images saved during computational modeling of wound healing is shown in Figs. 3 and 4. It was immediately apparent that the low-calcium model monolayer healed more quickly. Two of the three wounded monolayers (LW2 and LW3) were visually confluent after approximately 5 h, and LW1 reached confluence approximately 8 h after wounding, whereas none of the wounds in physiological [Ca^{2+}] had healed after 20 h of simulated time postwounding. Inspection of Figs. 3 and 4 revealed that the mechanism of healing differed between the two [Ca^{2+}] environments. Cells in the low-[Ca^{2+}] model migrated freely into the denuded area, whereas in the case of the physiological model, the wound edge moved as a contiguous sheet, and very few cells migrated individually into the wound. The stored JPEGs were linked together to produce virtual time-lapse movies of computational wound healing. Close inspection of these revealed further details about the mechanisms involved in wound closure. In the relatively low cell density wound model (LW1), the wound was closed almost entirely due to migration of individual cells into the wound, whereas in the higher density models, two "fronts" of cell movement were visible: cells at the leading edge migrated into the wound area, with a second, almost contiguous mass of cells that gradually encroached into the wound area due to the force created by cells spreading and proliferating behind. This latter mechanism was the sole factor driving wound closure in the higher [Ca^{2+}] model, and was much slower due to the higher level of quiescence in these models.

Locations of all virtual cells were recorded at every iteration "postwounding" in order that directly analogous results to the *in vitro* assay could be obtained. The number of cells within a 840-μm length of the original wounded area (equivalent to the field of view in the digital micrographs) was calculated, and results are shown for the low and physiological calcium models in Fig. 5. This figure illustrates that wound closure was significantly faster in low [Ca^{2+}], and also that in this environment in particular, the rate of closure appeared to be governed by the density of the cell population prior to wounding. Inspection of this figure suggests that wound closure in low-calcium models LW2 and LW3 (i.e., higher cell number and quiescence at wounding) is a biphasic process, with the original rapid increase in the number of cells in the wound area caused by migration (0–4 h), and the second increase (12–15 h) caused by proliferation. This behavior was not seen in the 2-mM [Ca^{2+}] model, where only the cells immediately adjacent to the wound edge were released from contact inhibition and reentered the cell cycle.

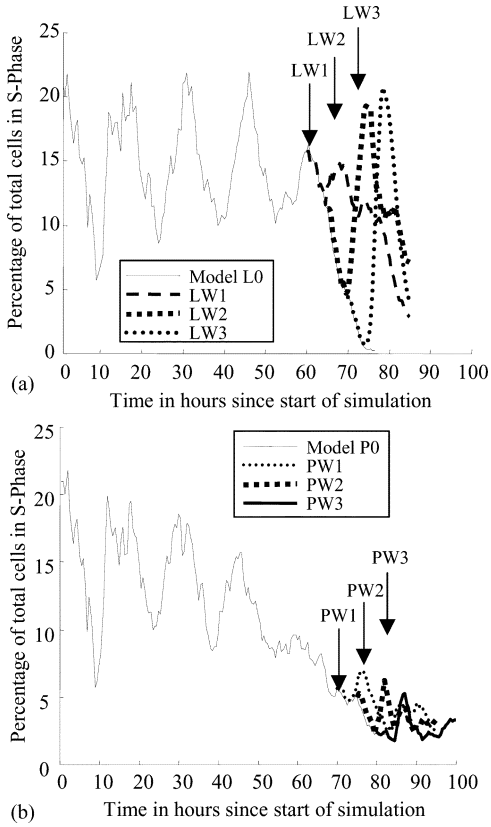

Fig. 6. S-phase cell population in wounded and nonwounded models in: (a) low-calcium and (b) physiological calcium environments. Arrows indicate points where nonwounded models were saved and virtual wounds created. (a) Time in hours since start of simulation. (b) Time in hours since start of simulation.

Quantitative analysis of the rate of wound closure in the low and physiological calcium computational models where wounds were created at 70 h postseeding (models LW3 and PW1), showed that closure in the physiological calcium model was delayed by 95% in the hour immediately following wounding, decreasing to a 60%–65% delay 11 h later.

2) Cell Proliferation: The number of cells in each phase of the cell cycle was saved at every iteration of each model, both with and without wounding. The percentage of the total cell population in S-phase at any point in time is shown in Fig. 6. In all models, this percentage was observed to be oscillatory, with a period of the mean cell cycle length (30 iterations or 15 h) and a mean value, for proliferative populations of approximately 15%, irrespective of [Ca^{2+}] and wounding. Possible explanations for this nonintuitive behavior are discussed in Section IV.

After approximately four cell cycles, there was a gradual decline in the proportion of S-phase cells. This reduction occurred more rapidly in physiological [Ca^{2+}] models, corresponding to

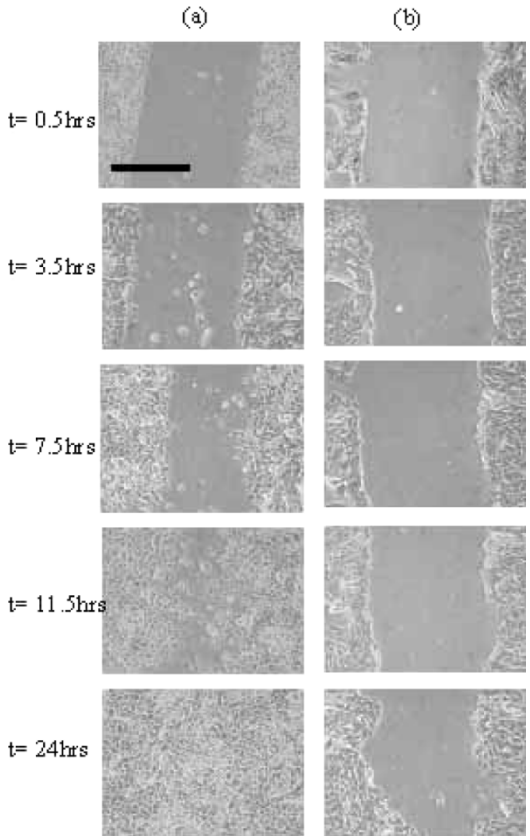

Fig. 7. Digital photographs illustrating wound closure behavior typical of NHU Y358 monolayers grown in: (a) low and (b) physiological calcium environments. Scale bar represents 500 μm.

an increased proportion of quiescent cells due to contact inhibition (cells with four or more intercellular bonds become contact inhibited and enter G0). Although there was some contact inhibition in the low-calcium models due to transient bonds formed at high cell density, the "size inhibition" rule (i.e., a cell must have a spread radius of at least 1.5 times the spherical seed radius in order to progress through the G1-G0 checkpoint) was more important in inducing quiescence in cell populations in low [Ca^{2+}].

As shown in Fig. 6, the effect of wounding a cell population did not have an immediate effect on the number of S-phase cells, but resulted in an increase in the proportion of the population in S-phase (analogous to the fraction of cells incorporating BrdU in the *in vitro* assays) approximately 5 h later. The S-phase populations continued to follow a periodic pattern postwounding, with the "peak" in activity occuring approximately 10 h after wounding in low [Ca^{2+}], and 7 h postwounding in physiological [Ca^{2+}]. The difference in S-phase fraction in the wounded model versus the nonwounded control was dependent on the degree of quiescence at the time of wounding. The latter determined both the decline in S-phase activity in the nonwounded control, and also the number of cells that could be potentially released from G0 and reenter the cell cycle in the wounded models. Analysis of cell cycle data showed that only cells located along the wound edge were released from contact inhibition in the physiological calcium models, whereas in the low-calcium simulations, cells

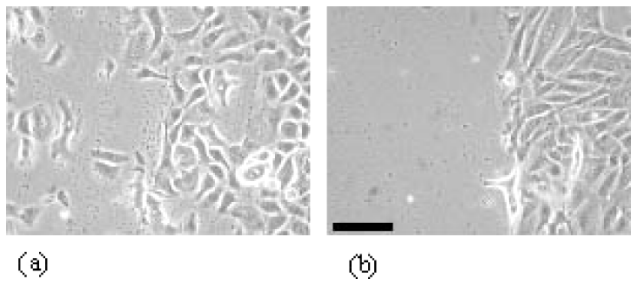

Fig. 8. Morphology of cells close to wound edge NHU cell line Y358, 11.5 h postwounding. (a) Low calcium, wound 2. (b) Physiological calcium, wound 2. Scale bar $= 100$ μm.

throughout the model gradually reentered the cell cycle (data not shown).

B. In Vitro Wounding

1) Wound Closure by Cell Migration: Fig. 7 shows a sequence of micrographs for typical scratch wound repairs in one low [Ca^{2+}] and one physiological [Ca^{2+}] well for NHU cell line Y358. Qualitative similarities between the behavior exhibited by the computational model and the real urothelial monolayer are apparent when these micrographs are compared to Figs. 3 and 4. In the case of the low-[Ca^{2+}] cultures, many individual cells can be observed migrating into the denuded area. Higher magnification micrographs showing typical cell morphology close to the wound edge in low and physiological calcium wells are shown in Fig. 8. In the low-calcium wells, isolated cells with ruffling membranes (lamellapodia) and long, thin cytoplasmic filapodial extensions protruding from the leading edges were visible. By contrast, cells cultured in physiological [Ca^{2+}] migrated into the wound as a confluent sheet.

The wound closure rates for cell line NHU Y358 obtained by counting the number of individual cells within the denuded area at each time point are shown in Fig. 9. In the case of the low-[Ca^{2+}] wells, one wound had closed within 12 h, and all three were closed 24 h postwounding. The rate of wound closure appeared to be exponential. Wounding was followed by a lag period of 2–3 h, during which there was no visible cell movement into the denuded area. Migration into the wound then commenced, resulting in coverage of the denuded area. The final cell number in the low-[Ca^{2+}] medium was related to the original width of the wound (see Table III), although the rate of wound closure appeared to be independent of this factor.

None of the wounds created under physiological [Ca^{2+}] conditions closed completely during the duration of the experiment, as illustrated by the significantly smaller final cell number. There was greater variation in the wound closure rate in 2 mM [Ca^{2+}], as indicated by the larger error bars. While there was a significant reduction in the area of wound 3, wound 1 barely closed at all during the course of the experiment. It can be seen that in the case of this cell line, the difference between the number of cells in the original wound area in physiological [Ca^{2+}] wells was approximately 50% of the number at the same time point in the low [Ca^{2+}], suggesting that the effect of the higher [Ca^{2+}] is to delay the wound healing process by approximately a factor of two.

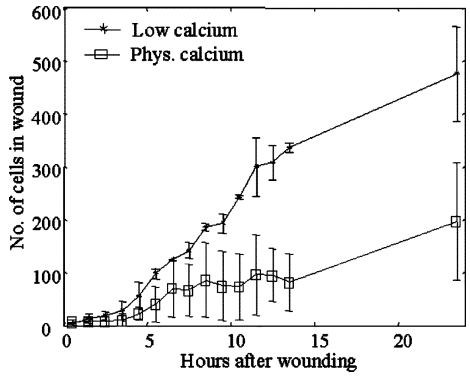

Fig. 9. Mean number of cells within original denuded area, manually counted from digital micrographs NHU cell line Y358. Error bars represent standard deviation calculated from three separate wounds.

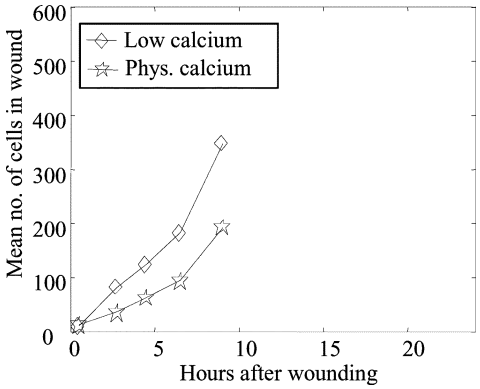

Fig. 10. Mean number of cells within original denuded area, manually counted from digital micrographs for NHU cell line Y388.

The process of manual cell counting was repeated at five time points between 0.5 and 9 h postwounding for NHU cell line Y388. In this case, wounds were made in duplicate monolayers at both low and physiological [Ca^{2+}]. As illustrated in Fig. 10, the wound closure rate was slightly quicker for this cell line, and all four wounds were observed to close completely within 24 h. However, the delay in closure of wounds in 2.0 mM [Ca^{2+}] relative to the cultures maintained in 0.09 mM [Ca^{2+}] was, again, approximately 50%.

When analyzing the digital micrographs, no distinction was made between cells migrating into the wound area from elsewhere in the monolayer and those resulting from the division of cells already present. However, inspection of the images showed very few mitotic cells, distinguishable as small, phase-bright, highly rounded objects. It was concluded that migration, as opposed to proliferation, was the dominant process responsible for the initial stages of wound closure in cultured urothelium.

2) Cell Proliferation: Proliferation indices were obtained at each time point by dividing the number of BrdU-labeled nuclei by the total number of nuclei, as revealed by Hoechst 33 258 staining. The mean proliferation indices for each time point are shown in Fig. 11.

An increase in BrdU incorporation was apparent in all plates, which did not return to the original level until approximately 30 h into the experiment. This universal change in the BrdU incorporation level, which we believe to be due to the replacement of the culture medium in both wounded and control plates at 0 h,

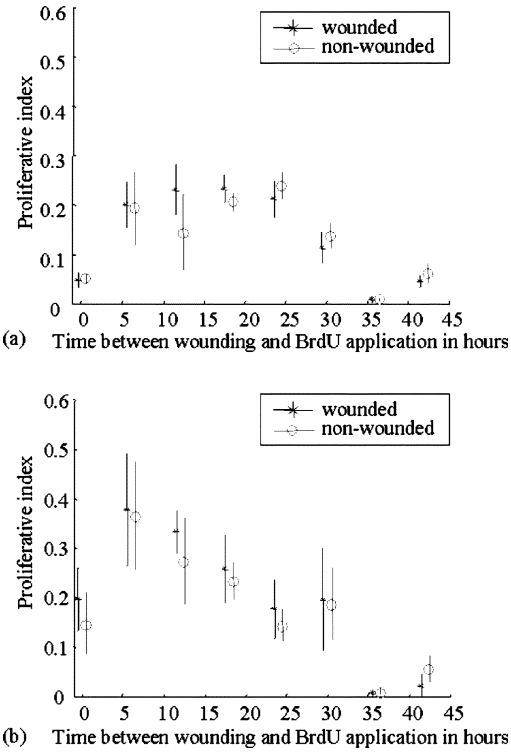

Fig. 11. Mean proliferative indices measured postwounding from cultures grown in media containing: (a) low and (b) physiological [Ca^{2+}]. (a) Time between wounding and BrdU application in hours. (b) Time beween wounding and BrdU application in hours.

makes separation of the effect due to wounding extremely difficult. The mean proliferation index measured in the low-[Ca^{2+}] plates during the first 30 h of the experiment was approximately 0.13, which corresponds well with that predicted by the computational model. However, in the case of the physiological [Ca^{2+}] plates, the mean index was significantly higher at 0.2. Very low levels of BrdU incorporation were observed at the 36-h time point in all plates. The most likely cause of this is believed to be experimental error. The oscillatory behavior predicted by the computational model was not apparent, although it is possible that this phenomenon was simply too subtle to measure using a labeling period of 6 h. Proliferation indices within each group were not normally distributed, so the nonparametric Mann–Whitney test was used to test the separation between wounded and nonwounded controls at each time point. Testing at the 95% confidence level yielded significant differences during the 12–18-h interval postwounding ($p = 0.045$ in low calcium and $p = 0.025$ in physiological calcium).

IV. Discussion

The development of computational models of biological systems is the first step toward obtaining tools that can be used to predict biological behavior, such as emergent tissue structure as the result of interactions between individual biological cells. The ability to carry out computational modeling of the wound healing process in parallel with *in vitro* assays has given us a valuable opportunity to assess the accuracy of the computational model in reproducing the behavior of biological cells, while also giving us a deeper insight into the mechanisms of monolayer

regeneration. We have developed our computational model using a software agent paradigm, in which biological cells are represented as individual autonomous entities with no higher level control system. This allows us to simulate concepts of self-assembly and emergent structure in biological tissues and also to examine how tissues respond to disruptions of the structure, as exemplified by scratch wounding of an epithelial monolayer.

Both *in vitro* and computational models indicate that wounded urothelial monolayers maintained in a low extracellular [Ca^{2+}] environment regenerate significantly more quickly than those maintained in physiological [Ca^{2+}]. In relatively dense cell populations maintained in low-[Ca^{2+}] environments, wound closure is a two-phase process: initially, individual cells migrate into the denuded area, while other cells are actively "pushed" into the wound by physical forces due to cell spreading and proliferation. After a period of at least 12 h, an increase in proliferation occurs, eventually resulting in a fully confluent monolayer. The magnitude of the effect of scratch wounding on the proliferative behavior of monolayers is strongly dependent on the density and degree of quiescence in the cell culture prior to wounding. In monolayers where the majority of cells are actively cycling, (e.g., model LW1), cells are replaced with minimal up-regulation of the background proliferation rate. In more quiescent cultures, the effect of wounding is the gradual recruitment of quiescent cells back into the cell cycle, which accounts for the increase of S-phase and mitotic activity discussed above. In our *in vitro* proliferation experiment and the computational model (which can be considered as a "virtual" BrdU assay), this increase of proliferation is manifested as a peak in S-phase activity approximately 10 h postwounding. The ability of an experimental assay to detect this increase in activity, relative to a nonwounded control, can be masked if activity in the control is up-regulated by other factors—in the case of the experiment presented here, the application of fresh culture medium to both the wounded and the control plates.

By contrast, migration of individual cells into the wound did not play a significant part in the wound healing process in a physiological [Ca^{2+}] environment. The forced removal of cells in the scratch wound will inevitably break some intercellular bonds, and a small number of cells immediately adjacent to the wound edge will reenter the cell cycle. The driving force to wound closure, at least in the computational models, is the "pushing" effect of cells growing and dividing. As many cells in these models are quiescent, this process takes significantly longer than in the low-calcium models.

The relatively small increase in proliferation, induced by the wounding of both the *in silico* and *in vitro* monolayers, is at odds with results reported by other workers. For instance, Chung *et al.* reported a 3.2–4.5-fold increase in proliferation of limbal and peripheral cells after creation of a 3-mm wound in the cornea [18]. Baskin *et al.* detected a six- to eightfold increase in transcription of keratinocyte growth factor and transforming growth factor alpha in full-thickness bladder tissue *in vivo*, 12–24 h after the creation of surgical wounds in rat bladders [19], although actual changes in proliferation in response to wounding were not examined during this study. In both these cases, fully differentiated tissue was used and the wounds were significantly larger than the 500–800-μm wounds considered here. It is possible that the proliferative response to wounding is directly related to the size of the wound. If the cells removed can be replaced within a relatively short period by the underlying proliferation in the tissue, it is unlikely that cells will be actively promoted to reenter the cell cycle. Investigation of the relationship between wound size and proliferative response would be an interesting area for future work.

The differences between experimental and computational models lie largely in the relative timing of events in response to wounding. Our computational model predicts that in monolayers maintained in low-[Ca^{2+}] medium, cell migration into the wounded area will occur immediately following wounding. As the wounded area is repopulated with cells, the migration rate will gradually decline. In the equivalent *in vitro* case, 3–4 h elapsed before cell migration occurred. This suggests either, or both, of the following possibilities: 1) in a confluent monolayer, cells may take a few hours to rearrange their cytoskeleton in order to commence migration and 2) cells migrate in response to a wound-induced signal (rather than simply "sensing" the reduction in cell density as they do in the computational model), which is not transmitted instantaneously. It is not possible to select either of these explanations on the basis of the results presented here, but experiments carried out by other workers have suggested the presence of a wound-induced signal in epithelial cells. For instance, Sammak *et al.* observed the propagation of an intracellular calcium signal in mouse mammary epithelial cultures immediately after wounding [20].

An absence of intercellular signaling may also be responsible for differences in growth characteristics between *in vitro* and *in silico* cell populations. In a previous study, we reported that NHU cell populations maintained *in vitro* in physiological [Ca^{2+}] actually expanded more quickly that those maintained in a low-[Ca^{2+}] medium during the first seven days after plating, whereas our computational model did not predict this behavior [6]. In the study reported here, we noted that the mean level of BrdU incorporation measured *in vitro* for both wounded and control cultures was higher than that predicted computationally. Nelson and Chen [15] recently used patterned substrates to demonstrate that intercellular signaling was an important factor in promoting growth in endothelial cells. It has also been shown that juxtacrine activation of EGF receptor-mediated pathways plays a critical role in controlling proliferation and differentiation of urothelial cells [4]. At present, cell agents in our computational model communicate only to share information concerning the presence of mutual intercellular bonds—there is no concept of intercellular signaling in response to stimuli such as wounding. These results suggest that intercellular signaling plays an important role in the self assembly of epithelial tissue, and that inclusion of a juxtacrine signaling mechanism would increase the accuracy of our model.

The computational modeling described in this paper was designed to examine the effects of scratch wounding on epithelial monolayers. However, during the course of this study, examination of the model results yielded an interesting phenomenon relating to the normal growth of monolayers: the cyclic pattern of the percentage of the cell population in S-phase.

There are a number of contributory factors that could account for this nonintuitive periodic behavior in the model. Initially, the seed cells are randomly distributed throughout the cell cycle, with the exception that none are permitted to be in the mitotic, or M-phase, resulting in approximately 15%–20% of the seeded population being in S-phase. As the simulation progresses, these cells will start to progress to the G2 phase. However, the model includes a "size inhibition" rule, which states that a cell must have a spread radius of at least 1.5 times the spherical seed radius in order to progress through the G1–G0 checkpoint. During the first few model iterations, cells have not had adequate time to spread sufficiently to meet this criterion and are, thus, delayed in G0 phase, resulting in more cells leaving S-phase than cells entering. In addition, after a few iterations, cells that were initially close to the end of the G2 phase will divide and produce daughters, but it will take approximately half the mean cycle time for these cells to reach S-phase. Thus the S-phase population, as a proportion of the total cell number, will progressively decrease until the first of these daughter cells leave G1, and this fraction will begin to rise again. This pattern will continue until a significant number of cells are delayed in G0, whereupon the S-phase population will eventually decrease to zero.

It is known that partial synchrony can occur in real cell populations if a significant proportion of the population is in G0 at the time of plating, for instance, due to contact inhibition. This synchrony is gradually lost through successive cycles due to other factors that introduce heterogeneity into the cell cycle time. For the relatively short time scales and cell numbers represented by our computational model, this synchronous behavior remains undiminished.

In order to determine whether synchrony persists for *in vitro* cell populations over periods of the order of days, it would be an interesting exercise to carry out BrdU or thymidine incorporation assays with a much shorter labeling period than is currently used (i.e., approximately 1 h). As the magnitude of the oscillations predicted by the model are relatively small (i.e., between 10% and 20% of the population total), and this would be expected to be even smaller for populations of millions of cells, all experimental parameters would have to be very tightly controlled in order to allow these small variations to be detected. This is an example of how even very simple computational modeling can raise questions concerning the characteristics of real biological systems.

V. Conclusion

We have carried out *in silico* simulations and *in vitro* experiments in order to test the ability of an agent-based computational model to simulate the self-assembly/repair characteristics of epithelial tissue. In particular, we have used this model, in parallel with *in vitro* assays, in order to investigate the influence of environmental $[Ca^{2+}]$ on the wound response of confluent urothelial cell monolayers Both modeling and experimental results show that cells in low-$[Ca^{2+}]$ environments rapidly migrate into the wound, whereas cells in physiological $[Ca^{2+}]$ migrate as a confluent sheet, with wound coverage occurring at about half the rate. Modeling also suggests that in confluent, quiescent cultures maintained in low-$[Ca^{2+}]$ medium, scratch wound repair may be associated with an increase in the proportion of cells entering the mitotic cycle.

We have shown that a simple agent-based model can make qualitatively accurate predictions about cell behavior in low- and high-$[Ca^{2+}]$ cultures based on two simple premises.

- Cells form more intercellular bonds in physiological $[Ca^{2+}]$.
- Intercellular bonds inhibit migration and eventually proliferation.

We have demonstrated that even this relatively simple model based on cellular interactions, including intercellular bonding, contact inhibition, and repulsive forces due to cell growth and division can simulate the wound response of confluent monolayers. We hypothesize that disparities in behavior of the *in vitro* and *in silico* models can be primarily attributed to the absence of intercellular signaling or subcellular-scale phenomena, such as intracellular signaling pathways and explicit cytoskeletal structure. We anticipate that future development of our computational model to replace empirical rules with models of pathways related to cell–cell and cell–environment interactions, such as EGF receptor-, integrin-, and E-cadherin-mediated cascades, will significantly improve the accuracy of our model in predicting real cell behavior.

References

[1] J. Southgate, K. R. Hutton, D. F. M. Thomas, and L. K. Trejdosiewicz, "Normal human urothelial cells *in vitro*: Proliferation and induction of stratification," *Lab. Invest.*, vol. 71, pp. 583–594, 1994.

[2] J. Southgate, P. Harden, P. J. Selby, D. F. M. Thomas, and L. K. Trejdosiewicz, "Culture of human urothelium," in *Culture of Epithelial Cells*, R. I. Freshney and M. G. Freshney, Eds. New York: Wiley, 2002.

[3] ——, "Urothelial tissue regulation: Unravelling the role of the stroma," *Adv. Exp. Med. Biol.*, vol. 462, pp. 19–30, 1999.

[4] C. L. Varley, J. Stahlschmidt, W.-C. Lee, J. Holder, C. Diggle, P. J. Selby, L. K. Trejdosiewicz, and J. Southgate, "Role of PPAR γ and EGFR signalling in the urothelial terminal differentiation programme," *J. Cell Sci.*, vol. 117, pp. 2029–2036, 2004.

[5] S. D. Scriven, C. Booth, D. F. Thomas, L. K. Trejdosiewicz, and J. Southgate, "Reconstitution of human urothelium from monolayer cultures," *J. Urol.*, vol. 158, pp. 1147–1152, 1997.

[6] D. C. Walker, J. S. Southgate, G. Hill, M. Holcombe, D. R. Hose, S. M. Wood, S. Macneil, and R. H. Smallwood, "The epitheliome: Modeling the social behavior of cells," *Biosystems*, 2003, to be published.

[7] H. Hennings and K. A. Holbrook, "Calcium regulation of cell–cell contact and differentiation of epidermal cells in culture," *Exp. Cell Res.*, vol. 143, pp. 127–142, 1983.

[8] J. Southgate, W. Kennedy, K. A. R. Hutton, and L. K. Trejdosiewicz, "Expression and *in vitro* regulation of integrins by normal human urothelial cells," *Cell Adhes. Commun.*, vol. 3, pp. 231–242, 1995.

[9] A. I. Magee, N. A. Lytton, and F. M. Watt, "Calcium-induced changes in cytoskeleton and motility in cultured human keratinocytes," *Exp. Cell Res.*, vol. 172, pp. 43–53, 1987.

[10] P. K. A. Jensen, J. O. R. Norgand, C. Knudsen, V. Nielsen, and L. Bolund, "Effects of extra- and intracellular calcium concentration on DNA replication, lateral growth, and differentiation of human epidermal cells in culture," *Virchows Arch. B, Cell Pathol. Incl. Mol. Pathol.*, vol. 59, pp. 17–25, 1990.

[11] B. St. Croix, C. Sheehan, J. W. Rak, V. A. Florenes, J. M. Slingerland, and R. S. Kerbel, "E-Cadherin-dependent growth suppression is mediated by the cyclin-dependent kinase inhibitor p27 KIPI," *J. Cell Biol.*, vol. 142, pp. 557–571, 1998.

[12] A. Stockinger, A. Eger, J. Wolf, H. Beug, and R. Foisner, "E-Cadherin regulates cell growth by modulating proliferation-dependent beta-catenin transcriptional activity," *J. Cell Biol.*, vol. 154, pp. 1185–1196, 2001.

[13] K. Takahashi and K. Suzuki, "Density-dependent inhibition of growth involves prevention of EGF receptor activation by E-Cadherin mediated cell–cell adhesion," *Exp. Cell Res.*, vol. 226, pp. 214–222, 1996.
[14] H. Chen, N. E. Paradies, M. Fedor-Chaiken, and R. Brackenbury, "E-Cadherin mediates adhesion and suppresses cell motility via distinct mechanisms," *J. Cell Sci.*, vol. 110, pp. 345–356, 1997.
[15] C. M. Nelson and C. S. Chen, "Cell-cell signalling by direct contact increases cell proliferation via a P13K-dependent signal," *FEBS Lett.*, vol. 514, pp. 238–242, 2002.
[16] C. M. Adams, Y. T. Chen, S. J. Smith, and W. J. Nelson, "Mechansims of epithelial cell–cell adhesion and cell compaction revealed by high-resolution tracking of E-Cadherin-green flourescent protein," *J. Cell Biol.*, vol. 142, pp. 1105–1119, 1998.
[17] W. Baumgartner, P. Hinterdorfer, W. Ness, A. Raab, D. Vestweber, H. Schindler, and D. Drenckhahn, "Cadherin interaction probed by atomic force microscopy," *Proc. Nat. Acad. Sci.*, vol. 97, pp. 4005–4010, 2000.
[18] E.-H. Chung, A. E. K. Hutcheon, N. C. Joyce, and J. D. Zieske, "Synchronization of the G1/S transition in response to corneal debridement," *Invest. Opthalmol. Vis. Sci.*, vol. 40, pp. 1952–1958, 1999.
[19] L. S. Baskin, R. S. Sutherland, A. A. Thomson, H. T. Nguyen, D. M. Morgan, S. W. Hayward, Y. K. Hom, M. DiSandro, and G. R. Cunha, "Growth factors in bladder wound healing," *J. Urol.*, vol. 157, pp. 2388–2395, 1997.
[20] P. J. Sammak, L. E. Hinman, P. O. T. Tran, M. D. Sjaasad, and T. E. Machen, "How do injured cells communicate with the surviving cell monolayer?," *J. Cell Sci.*, vol. 110, pp. 465–475, 1997.

D. C. Walker, photograph and biography not available at the time of publication.

G. Hill, photograph and biography not available at the time of publication.

S. M. Wood, photograph and biography not available at the time of publication.

R. H. Smallwood, photograph and biography not available at the time of publication.

J. Southgate, photograph and biography not available at the time of publication.